Maximization of Underwater Sensor Networks Lifetime via Fountain Codes

Huseyin Ugur Yildiz, *Member, IEEE*

***Abstract*—The severe nature of underwater channel poses a great challenge for prolonging Underwater Acoustic Sensor Networks (UASNs) lifetime and achieving a reliable communication performance. Traditional approaches to improve the reliability such as automatic repeat request (ARQ) negatively affect the network lifetime (NL) due to energy dissipation caused by ARQ retransmission. A forward error correction (FEC) technique called Fountain codes (FCs) can solve the energy efficiency problem of ARQ by transmitting both the original packet and some redundant packets to ensure a targeted reliability with few or no retransmissions. In this work, we investigate performances of both traditional ARQ and FC based FEC methods in terms of NL, end-to-end delay, energy consumption, and frame error rate (FER) for UASNs. In this context, we abstract energy dissipation characteristics of conventional ARQ and FC based FEC method at the link-layer. We propose an integer linear programming (ILP) framework that maximizes the NL which is operated on top of developed link-layer energy consumption models. Our results reveal that FC based FEC methods can prolong the NL at a minimum of 16% while end-to-end delay, energy consumption, and FER can be reduced at least by 11%, 14%, and 9% as compared to classical ARQ, respectively.**

***Index Terms*—underwater acoustic sensor networks, network lifetime, automatic repeat request, fountain codes, integer linear programming.**

.

I. Introduction

UNDERWATER Acoustic Sensor Networks (UASNs) are used in a vast range of commercial and military aquatic applications [1]–[4]. UASNs use sound (acoustic) waves for communications where acoustic waves are characterized by limited bandwidth, large propagation delay, high attenuation, *etc.* [5]. UASN nodes have scarce energy sources and they consume excessive energy [6]. It is practically infeasible to replace the batteries of underwater nodes [7]. Hence, providing a reliable communication performance for a prolonged network lifetime (NL) is a challenging research topic in UASNs.

In UASNs, transmission errors over long acoustic links are inevitable [8]. There are mainly two approaches to improve the reliability of acoustic links in UASNs [9]. The first method is called plain *Automatic Repeat reQuest (ARQ)* where each successfully transmitted packet is acknowledged with a feedback packet (*i.e.*, acknowledgement (ACK) packet). Although plain ARQ method can guarantee the reliability, this technique is not energy efficient since retransmissions are required whenever an error is occurred in either data or ACK packets, which increases the energy consumption of nodes [10]. Moreover, due to the speed of sound waves in water, plain ARQ approach significantly increases the end-to-end delay (*i.e.*, time elapsed for a data packet to traverse from a source node to the sink node) especially in sparsely deployed UASNs [11].

The second approach to improve the reliability of underwater channel is the *Forward Error Correction (FEC)* which reduces the number of retransmissions as compared to plain ARQ [12]. *Fountain Code (FC)* [13] is considered as a prominent FEC method that can be used in UASNs [14]. In FCs, a group of M original message packets are encoded into $N \geq M$ bulk packets to be transmitted. The receiving node can recover the original data packet with high probability as soon as it receives M packets out of N packets [15], [16]. Although FCs may not fully ensure the reliability as plain ARQ, they can help to reduce the end-to-end delay since less or no retransmissions are required as compared to plain ARQ. Moreover, FCs have the advantage of reducing the energy consumption of nodes since the number of retransmissions required for FCs is less than plain ARQ [17].

In literature, FCs and other types of FEC methods are used together with ARQ (*i.e.*, hybrid ARQ) for reliable data transportation in UASNs (*e.g.*, [5], [9], [12], [14], [15], [18]–[22]). The proposed approaches in the literature require feedback channels which have negative impacts on both the end-to-end delay and the NL. Such negative impacts can be mitigated if feedback channels are ignored (*e.g.*, [8], [10], [17], [23]). Yet, performances of proposed FC based hybrid transmission schemes are explored in terms of throughput, delay, energy efficiency, reliability, *etc.* However, the impact of FC based FEC transmission methods on UASN NL as compared to plain ARQ remains unclear. Our main contributions are enumerated as follows:

1) We develop two link-layer energy consumption models called "Plain FC" (*i.e.*, FCs without feedback channels) and "FC-ARQ" (*i.e.*, FCs with feedback channels) to abstract FC based FEC transmission methods presented in the literature by using the power consumption characteristics of the Woods Hole Oceanographic Institution (WHOI) Micromodem [24] which is a popular underwater modem platform preferred in many aquatic research. In order to assess the performance of plain FC and FC-ARQ, we also abstract the energy consumption of plain ARQ scheme which is used as a benchmark.
2) Developed link-layer models are bolstered with an adap-

H. U. Yildiz is with the Department of Electrical and Electronics Engineering, TED University, 06420, Ankara, Turkey (e-mail: hugur.yildiz@tedu.edu.tr).

tive transmission power adjustment method that satisfies a certain link quality by considering the fundamental principles of underwater propagation at the physical layer.
3) We propose an integer linear programming (ILP) framework that maximizes the NL which is operated on top of link-layer energy abstraction models.
4) By using the ILP framework, we compare the NL as well as corresponding end-to-end delay, energy consumption, and frame error rate (FER) performances of plain FC and FC-ARQ strategies to plain ARQ under a large set of network configurations and reliability criteria.

The remaining part of the paper proceeds as follows. Section II overviews the literature on the usage of FCs in UASNs. Developed link-layer energy abstraction models and the ILP framework are presented in Section III. Performance evaluation of the proposed strategies is elaborated in Section IV. Finally, Section V provides conclusions of this work.

II. Related Work

The issue of reliable data transfer has received considerable critical attention in UASNs literature. A recent survey on reliable data transfer schemes proposed for UASNs is given in [25]. Another survey in [26] provides a comprehensive review on energy-efficient, reliable medium access control (MAC), and routing protocols in UASNs. The performance of reliable transfer protocols for UASNs can be enhanced by using channel coding techniques [27].

There is a large volume of published studies on the usage of FCs in underwater networks that focuses on the performance of proposed hybrid protocols (*i.e.*, protocols that combine FC with ARQ for reliable data transfer). Fountain Code based Adaptive multi-hop Reliable (FOCAR) data transfer [5], FCs and Selective-Repeat ARQ scheme (FSR-ARQ) [9], and network coding based hybrid ARQ (NCHARQ) [14] are three examples of the proposed FC based hybrid protocols. In [18], [19], performances of FC based hybrid ARQ protocols are investigated for multicasting and broadcasting in underwater channels, respectively. In [20], an adaptive coding approach is developed which uses incremental redundancy hybrid ARQ (IR-HARQ) protocol to optimize the number of parity check symbols transmitted in a single packet transmission.

There are also a few studies available in the literature which use FCs or their practical realizations (*i.e.*, Luby Transform codes [28] or Raptor codes [29]) for data centric storage in UASNs (*e.g.*, [30]–[33]). Various studies have utilized random linear coding (RLC) which is a representative of FC for reliable data transports in UASNs. Underwater Hybrid ARQ (UW-HARQ) [12] is an example of a hybrid protocol that combines RLC with plain ARQ. In [15], an adaptive power control method using RLC is proposed for reducing the energy consumption in underwater channels. Moreover, in [21], a hybrid transmission method which employs both RLC and plain ARQ is developed to optimize the number of transmitted packets to satisfy a targeted reliability at the receiver for underwater channels. In [22], authors combine the works in [15] and [21]. However, the number of encoded packets and transmission powers are determined by using the channel state information which is obtained via the feedback channel. On the other hand, hybrid utilization of FCs with other type of FEC codes (*e.g.*, block and convolutional codes) is also implemented for reliable data deliveries in UASNs (*e.g.*, [11], [17], [34]). Improvements of FC encoding and decoding algorithms are investigated for UASNs in [35].

Existing studies on FC based data transfer approaches mentioned above require a feedback channel to ensure predefined reliability criteria. We can classify these studies (*e.g.*, [5], [9], [11], [12], [14], [15], [18]–[22], [30]–[34]) as "FC-ARQ" strategies. On the other hand, in [17], an encoding scheme is proposed where FEC and FCs are utilized together without using feedback channels. In [10], authors propose a digital FC called Recursive Luby Transform Code (RLT) and develop the RLT Code based Handshake-Free (RCHF) protocol. In [23], an experimental study on the usage of FCs is performed for UASNs. The number of required transmissions to achieve the targeted FER is extensively investigated without using feedback channels. A stochastically optimized Raptor code based transmission scheme without feedback channels is proposed in [8]. Proposed methods which do not require a feedback channel in the reviewed studies (*e.g.*, [8], [10], [17], [23]) can be classified as "plain FC" strategies.

Recently, researchers have shown an increased interest in NL maximization techniques by using optimization methods for sensor networks. One of the most popular objective functions for the NL maximization is to minimize the reciprocal of the NL [36], [37]. Another popular objective function is the direct maximization of the NL (which is adopted in this work) to determine an optimum data flow routing plan for nodes to convey their data to the base station [37], [38]. Nonetheless, in both objective functions, maximization of the lifetime of the node which has the minimum lifetime should be aimed. In this way, sensor nodes collaborate to avoid the premature death of any individual node such that sensor nodes dissipate their battery energies in a balanced fashion. We refer the interested reader to recently published surveys on other types of NL maximization techniques which are detailed in [36]–[39].

The most related studies to our work are presented in [6], [7] where energy consumption characteristics of FCs in UASNs are explored. In [6], an FC based protocol with feedback channel is proposed that dynamically adjusts the encoding scheme by considering the residual energy of the transmitter and receiver for maximizing the number of messages exchanged by nodes. In [7], energy consumption analysis of FCs is investigated without using feedback channels.

Unlike the existing works presented in the literature, to the best of our knowledge, this is the first study that compares two generic abstractions of FC based FEC methods (*i.e.*, plain FC and FC-ARQ) to the plain ARQ in terms of NL, end-to-end delay, energy consumption, and FER via an ILP framework by considering a large set of reliability criteria and network configurations for UASNs. In fact, FC-ARQ and plain FC strategies employ the main design principles of two main FC based FEC approaches proposed in the literature while plain ARQ is the simplest method that is used in numerous studies for UASNs. One of our contributions in this study is to quantitatively compare the two prominent examples of FC

based FEC methods in the literature to plain ARQ strategy under optimum network operation conditions (*e.g.*, under same assumptions, scenarios, *etc.*) within a generic ILP framework.

III. System Model

In this section, we present the underwater channel model, energy dissipation models of FC-ARQ, plain FC, and plain ARQ; and ILP framework that maximizes the NL. Table I provides the nomenclature used in this paper.

A. Underwater Channel Model

We develop the underwater channel by using Urick's model where the attenuation of link-(i,j) (in dB) is calculated as [7]

$$\overline{A_{ij}} = \overline{A_0} + 10\kappa \log_{10}(d_{ij}) + d_{ij} \times 10^{-3} \times \overline{\alpha}, \quad (1)$$

where $\overline{A_0} = 30$ dB models the transmission anomaly (*i.e.*, multipath propagation, refraction, and other phenomena) [40], $\kappa = 2$ is the spherical spreading factor to simulate a severe underwater environment in deep waters [18], d_{ij} is the distance of the link-(i,j) (in meters), and $\overline{\alpha}$ is the absorption coefficient (in dB/km) that is calculated by using Thorp's equation as [7]

$$\overline{\alpha} = \frac{0.11 f^2}{1+f^2} + \frac{44 f^2}{4100+f^2} + 2.75 \cdot 10^{-4} f^2 + 0.003. \quad (2)$$

We approximate the power spectral density of the ambient noise (which consists of turbulence, shipping, waves, and thermal noises) as [7]: $\overline{NL} \approx 50 - 18\log_{10}(f)$. To calculate $\overline{A_{ij}}$, $\overline{\alpha}$, and $\overline{NL}$, we use $f = 25$ kHz which is the central operation frequency of WHOI Micromodem [24]. If we assume node-i and node-j to represent the transmitter and receiver nodes, respectively, the signal-to-noise ratio (SNR) at the receiver node-j (*i.e.*, $\overline{\gamma_{ij}(l)}$ in dB) is calculated as [9]

$$\overline{\gamma_{ij}(l)} = \overline{P_{SL}(l)} - \overline{NL} - \overline{A_{ij}} \geq \overline{\gamma_{tgt}}, \quad (3)$$

where $\overline{P_{SL}(l)}$ is the sound source level by using the power level-l (in dB re 1μPa) and $\overline{\gamma_{tgt}} = 20$ dB is the targeted SNR at the receiver [7]. The sound source level is given by [41]

$$\overline{P_{SL}(l)} = 10\log_{10}\left(\frac{P_{tx}(l)}{2\pi h I_0}\right), \quad (4)$$

where $I_0 = 0.67 \times 10^{-18}$ is the reference intensity [41], $h = 1000$ m is the depth of the water, and $P_{tx}(l)$ is the electrical transmission power at level-l (in Watts). Throughout this paper, we denote the set of power levels of WHOI Micromodem as $\mathcal{L}$ where $P_{tx}(l)$ varies between 8 W and 48 W [24]. For granularity, we assume that there are 11 discrete power levels available (*i.e.*, $\mathcal{L} = \{8 \text{ W}, 12 \text{ W}, \ldots, 48 \text{ W}\}$).

We consider a block fading model where the channel conditions are constant and known for a duration of over a transmission (*i.e.*, either a bulk of encoded frames transmission for FC based FEC methods or a single unencoded frame transmission as in plain ARQ) and changing for each new transmission [15], [22], [42]. This is a reasonable assumption since the underwater modem has a low data rate such that each transmission is sufficiently separated over time. As a result, each transmission will be exposed to independent fading [42]. For the non-coherent binary frequency shift keying (BFSK) modulation, the bit error rate (BER) for the uncoded modulation when considering a K-distributed fading channel is calculated as [17]

$$p_{ij}^B(l) = \frac{\nu}{\Gamma(\nu)} \int_0^\infty \frac{u^{\nu-1} e^{-u}}{2\nu + u\gamma_{ij}(l)} du, \quad (5)$$

where $\nu = 1.5$ is the shape parameter of K-distributed fading [7], $\Gamma(\cdot)$ is the Gamma function, and $\gamma_{ij}(l)$ is the SNR in ordinary form. For a frame with length φ bits, the FER is

$$p_{ij}^F(l,\varphi) = 1 - (1 - p_{ij}^B(l))^\varphi. \quad (6)$$

B. Data Link Layer Models

We assume a slotted communication scheme where the NL (*i.e.*, the time until the first node drains out its available battery [36]) is divided into equal durations of *rounds* such that each round lasts for $T_R = 100$ seconds (s) [20]. Each round has two phases, which are the active and hibernation phases. In the active phase, each sensor node generates a single flow (*i.e.*, a bulk of encoded frames for FC based FEC methods or a single unencoded frame as in plain ARQ) which is transmitted to the base station and ACKed back (except for plain FC). While waiting for an ACK frame, each sensor node switches to the idle mode. In plain ARQ, retransmissions are performed whenever there are errors in either data or ACK frames. In FC-ARQ, retransmissions are performed only for the dropped ACK frames. No retransmissions are required in plain FC. The hibernation phase starts as soon as generated flows of sensor nodes are successfully collected at the base station and this phase ends after 100 s. In each round, sensor nodes dissipate energy in both the active and hibernation phases. Channel conditions are assumed to be constant in a single round due to the block fading and changing for each round. Rounds are repeated until the first sensor node depletes its battery energy.

Generated data frames are $L_P = 1024$ bits [17]. Some applications that are adopting 1024 bits of frame sizes include connectivity [43], energy hole avoidance [44], NL-aware data gathering [45], data collection via autonomous underwater vehicles [40], and channel coding [17]. In Section IV, we also consider using shorter frame sizes. For FC-ARQ and plain ARQ strategies, we use a single ACK frame of size $L_A = 64$ bits [40]. For plain FC strategy, no ACK packets are transmitted.

1) FC-ARQ: In FC-ARQ, the original data frame of size L_P bits is divided into M smaller sections of size L_P/M bits which are encoded into $N \geq M$ frames to be transmitted from node-i to node-j by using the power level-l at each round. At node-j, the success probability of FC is calculated as [7]

$$P_{ij}^s(l) = \sum_{m=M}^{N} \binom{N}{m} (1 - p_{ij}^F(l, L_P))^m (p_{ij}^F(l, L_P))^{N-m}. \quad (7)$$

This equation calculates the probability that at least M frames are successfully received. To ensure a predetermined reliability, $P_{ij}^s(l)$ should be greater than a targeted reliability criterion. FC-ARQ determines the minimum value of N (*i.e.*, $N_{ij}^*(l)$) that satisfies $P_{ij}^s(l) \geq P_{tgt}^*$, $\forall l \in \mathcal{L}$, $\forall i$, $\forall j$

TABLE I: List of symbols and their descriptions used in this paper.

Symbol	Description	Symbol	Description
$\overline{\alpha}$	Absorption coefficient (dB/km) [7]	$\overline{A_{ij}}$	Attenuation of link-(i,j) (dB) [7]
$\overline{A_0}$	Transmission anomaly (30 dB) [40]	$\overline{NL}$	Power spectral density of the ambient noise (dB) [7]
$\overline{P_{SL}(l)}$	Sound source level by using the power level-l (dB re 1μPa) [41]	$\overline{\gamma_{ij}(l)}$	SNR at the receiver node-j (dB) [9]
$\overline{\gamma_{tgt}}$	Targeted SNR at the receiver (20 dB) [7]	β	Integer variable that shows the total hop count in the network
β^*	Total hop count in the network that maximizes the NL (parameter)	$\Gamma(\cdot)$	Gamma function
$\gamma_{ij}(l)$	SNR at the receiver node-j (ordinary form)	η_{ji}	Average number of transmissions required over link-(i,j)
κ	Spherical spreading factor (2) [18]	ν	Shape parameter of K-distributed fading (1.5) [7]
ξ	Initial battery of sensor nodes (100 KJ)	ρ	Efficiency of the microcontroller (0.95)
$\mathcal{E}$	Set of all directed links	$\mathcal{L}$	Set of power levels for WHOI Micromodem
$\mathcal{M}$	Sufficiently a large number used as an upper bound on flows	$\lvert W\rvert$	Number of sensor nodes (20)
$(E_{ij}^{tx})^*$	Optimum transmission energy cost over link-(i,j) (J)	$(E_{ji}^{rx})^*$	Optimum reception energy cost over link-(i,j) (J)
(l,k)	Transmission power levels for data and ACK frames	a_{ij}^m	Binary variable that shows whether the link-(i,j) conveys the frame originated at node-m or not
c	Nominal speed of sound in water ($\approx$ 1500 m/s) [18]	d_{ij}	Distance between node-i and node-j (m)
d_{net}	Network edge length (2–4 km)	$E_{adj}(M)$	The energy consumption to compute the adjugate of the recovering matrix (J) [6]
$E^{dec}(M)$	The energy dissipation for decoding the original message (J) [6]	$E_{det}(M)$	The energy consumption to compute the determinant of the recovering matrix (J) [6]
$E_{ij}^{enc}(l)$	Encoding energy cost for FC (J) [6]	$E_{rx,ji}^{HDS,f1}(l,k)$	Reception energy consumption for a failed handshake due to the case (ii) (J)
$E_{rx,ji}^{HDS,f2}(l,k)$	Reception energy consumption for a failed handshake due to the case (iii) (J)	$E_{rx,ji}^{HDS,s}(l,k)$	Reception energy consumption for a success handshake (J)
$E_{tx,ij}^{HDS,f}(l,k)$	Transmission energy consumption for a failed handshake due to the cases (ii) and (iii) (J)	$E_{tx,ij}^{HDS,s}(l,k)$	Transmission energy consumption for a success handshake (J)
E_i	Continuous variable that models the total energy dissipation of sensor node-i during the NL (J)	$E_{ji}^{rx}(l,k)$	Total reception energy dissipation over link-(i,j) in a single round (J)
$E_{ij}^{tx}(l,k)$	Total transmission energy dissipation over link-(i,j) in a single round (J)	f	Central operation frequency of WHOI Micromodem (25 kHz) [24]
f_{ij}^m	Integer variable that represents the number of flows originated from node-m which are transmitted over link-(i,j) through the NL	f_{mc}	Frequency of operation for the microcontroller of WHOI Micromodem (160 MHz) [24]
h	Depth of the water (1000 m)	I_0	Reference intensity (0.67×10^{-18}) [41]
l_{ij}^*	Optimum transmission power levels used for data frames over link-(i,j)	L_A	ACK frame size (64 bits) [40]
L_P	Data frame sizes (1024, 512, and 256 bits)	k_{ji}^*	Optimum transmission power levels used for ACK frames over link-(j,i)
M	Number of small packets to be encoded for FC	N	Total number of encoded packets to be transmitted for FC
$N_{ij}^*(l)$	Minimum number of encoded packets to be transmitted for FC satisfying $P_{ij}^s(l) \geq P_{tgt}^*$	N_R	Free variable that models the NL (in rounds)
$p_{ij}^B(l)$	Bit error probability over link-(i,j) when using transmission power level-l	$p_{ij}^F(l,\varphi)$	FER of a frame of size φ which is transmitted with power level-l over link-(i,j)
$p_{ij}^{HDS}(l,k)$	Probability of a successful handshake	P_{tgt}^*	Targeted success delivery probability of FC encoded packets (0.8, 0.9, and 0.999) [17]
P_{hbr}	Power required for WHOI Micromodem to stay in hibernation phase (220 μW) [24]	P_{mc}	Power consumption for the microcontroller of WHOI Micromodem (180 mW) [24]
P_{rx}	Reception power of WHOI Micromodem (1 W) [7]	$P_{ij}^s(l)$	Success probability of FC over link-(i,j) by using power level-l
P_{std}	Idle power consumption of WHOI Micromodem (80 mW) [24]	$P_{tx}(l)$	Electrical transmission power at level-l (W)
R	Data rate of WHOI Micromodem (5 kbps) [24]	R_{max}	Maximum transmission range of sensor nodes (2.5 km) [9]
$(t_{ij}^s)^*$	Optimum slot time of the active phase for link-(i,j) (s)	t_A	Transmission time of an ACK frame of size L_A bits (s)
t_{ij}^d	Propagation delay of link-(i,j) (s)	t_D'	Transmission time of a data frame of size L_P bits (s)
t_D	Transmission time of a data frame of size L_P/M bits (s)	$t_{ij}^s(l,k)$	Slot time of the active phase when using power levels (l,k) for data and ACK frames over link-(i,j) (s)
T_{act}^i	Total active phase duration of node-i during the NL (s)	T_R	Round duration (100 s) [20]
V	Set of all nodes (including the base station, node-1)	W	Set of all sensor nodes (excluding the base station, node-1)

where P_{tgt}^* is the targeted success delivery probability of FC encoded packets and l is the discrete power level used on link-(i,j) which is chosen from the set $\mathcal{L}$ (*i.e.*, the set of power levels for WHOI Micromodem). We assume that the SNR information is passed to the transmitter by using ACK frames after each bulk of encoded frames transmission [22]. If ACK frames have errors, then $N_{ij}^*(l)$ values that satisfy a predetermined reliability criterion for the next bulk of encoded frames transmission cannot be determined precisely. Note that, $N_{ij}^*(l)$ depends on the FER information (*i.e.*, $p_{ij}^F(l,L_P)$) which is a function of the BER (*i.e.*, $p_{ij}^B(l)$), consequently, the SNR (*i.e.*, $\gamma_{ij}(l)$). Since the SNR information changes for each bulk of encoded frames transmission, FC-ARQ strategy relies on successful reception of ACK frames to calculate subsequent $N_{ij}^*(l)$ values accurately. The slot time of the active phase for FC-ARQ is calculated as

$$t_{ij}^s(l,k) = N_{ij}^*(l)t_D + t_{ij}^d + (t_{ji}^d + t_A) \times \eta_{ji}(k). \quad (8)$$

In this equation, $t_D = \frac{L_P/M}{R}$ and $t_A = \frac{L_A}{R}$ are the transmission times of a data frame (of size L_P/M bits) and

an ACK frame, respectively, where $R = 5$ kbps is the data rate of WHOI Micromodem [24]. $t_{ij}^d = \frac{d_{ij}}{c}$ is the propagation delay of link-(i,j) where $c \approx 1500$ m/s is the nominal speed of sound in water [18]. The term, $\eta_{ji}(k) = \frac{1}{1-p_{ji}^F(k,L_A)}$, accounts for the average number of transmissions required for ACK frames to be successfully received at node-i where $p_{ij}^F(k,L_A)$ is the FER of the ACK frame which is transmitted from node-j to node-i with power level-k. As a summary, in each round, a bulk transmission of $N_{ij}^*(l)$ number of data frames is performed by node-i where this bulk transmission lasts $N_{ij}^*(l)t_D$ s. The bulk transmission experiences a single propagation delay of t_{ij}^d s. On the other hand, an ACK frame is sent by the receiver node-j where the ACK frame may encounter errors in the reverse feedback channel. Considering the retransmissions, the ACK frame is successfully received by the transmitter node-i at most in $(t_{ji}^d + t_A) \times \eta_{ji}(k)$ s, on the average.

The transmitter node-i consumes $P_{tx}(l)N_{ij}^*(l)t_D$ of energy for transmitting $N_{ij}^*(l)$ number of data frames by using the power level-l over link-(i,j). After the bulk transmission of data frames, node-i switches to the idle mode to wait for an ACK frame for a duration of $[t_{ij}^s(l,k) - N_{ij}^*(l)t_D - t_A\eta_{ji}(k)]$ s. In this period, node-i spends $P_{std}[t_{ij}^s(l,k) - N_{ij}^*(l)t_D - t_A\eta_{ji}(k)]$ of energy to stay in the idle mode where $P_{std} = 80$ mW is the power cost of WHOI Micromodem to stay in the idle mode [24]. Finally, node-i dissipates an average energy of $P_{rx}t_A\eta_{ji}(k)$ for receiving the ACK frame including retransmissions where $P_{rx} = 1$ W is the reception power of WHOI Micromodem [7]. The encoding energy cost for FC at the transmitter node-i is calculated by using the derivations presented in [6] as

$$E_{ij}^{enc}(l) = [12 + 4L_P N_{ij}^*(l)]\frac{P_{mc}}{f_{mc}\rho}, \tag{9}$$

where $P_{mc} = 180$ mW is the power consumption and $f_{mc} = 160$ MHz is the frequency of operation for the microcontroller of WHOI Micromodem [24]. $\rho = 0.95$ is assumed to the efficiency of the microcontroller. Thus, the total energy dissipation of transmitter node-i in a single round is expressed as

$$\begin{aligned} E_{ij}^{tx}(l,k) = {} & E_{ij}^{enc}(l) + P_{tx}(l)N_{ij}^*(l)t_D + P_{rx}t_A\eta_{ji}(k) \\ & + P_{std}[t_{ij}^s(l,k) - N_{ij}^*(l)t_D - t_A\eta_{ji}(k)]. \end{aligned} \tag{10}$$

On the other hand, the receiver node-j consumes at most $P_{rx}N_{ij}^*(l)t_D$ of energy for receiving $N_{ij}^*(l)$ number of data frames which are transmitted by node-i with power level-l. Moreover, $P_{tx}(k)t_A\eta_{ji}(k)$ of energy is consumed for transmitting an ACK frame with power level-k including retransmissions on the average. The receiver node-j stays in the idle mode if it does not transmit an ACK frame or receive data frames. Hence the total time that node-j stays in the idle mode is at least $[t_{ji}^s(l,k) - N_{ij}^*(l)t_D - t_A\eta_{ji}(k)]$ s. The energy consumption in this case can be expressed as $P_{std}[t_{ji}^s(l,k) - N_{ij}^*(l)t_D - t_A\eta_{ji}(k)]$. The energy dissipation for decoding the original message is calculated as [6]

$$\begin{aligned} & E^{dec}(M) = \\ & [4L_P M + 14M^2 + E_{det}(M) + E_{adj}(M)]\frac{P_{mc}}{f_{mc}\rho}, \end{aligned} \tag{11}$$

where $E_{det}(M)$ and $E_{adj}(M)$ are energy consumptions to compute the determinant and the adjugate of the recovering matrix, respectively. $E_{det}(M)$ and $E_{adj}(M)$ are recursively calculated in the following two equations [6]

$$E_{det}(M) = [4M + ME_{det}(M-1)]\frac{P_{mc}}{f_{mc}\rho}, \tag{12}$$

$$E_{adj}(M) = M^2[12 + E_{det}(M-1)]\frac{P_{mc}}{f_{mc}\rho}. \tag{13}$$

Hence, the total energy consumption of receiver node-j in a single round is given as

$$\begin{aligned} E_{ji}^{rx}(l,k) = {} & E^{dec}(M) + P_{tx}(k)t_A\eta_{ji}(k) + P_{rx}N_{ij}^*(l)t_D \\ & + P_{std}[t_{ji}^s(l,k) - N_{ij}^*(l)t_D - t_A\eta_{ji}(k)]. \end{aligned} \tag{14}$$

2) Plain FC: The idea of plain FC is similar to FC-ARQ with the exception on the usage of feedback channels. The number of encoded data frames to be sent over each link (*i.e.*, $N_{ij}^*(l)$) is set a priori before transmission [23]. Thus, $N_{ij}^*(l)$ values are assumed to be determined via Eq. (7) by the base station in a centralized manner. In this strategy, ACK frame transmissions in the feedback channel are eliminated (*i.e.*, $t_A = 0$). Hence, the slot time of the active phase for plain FC is modified from Eq. (8) as

$$t_{ij}^s(l,k) = N_{ij}^*(l)t_D + t_{ij}^d. \tag{15}$$

In this equation, the total propagation delay is reduced from $2t_{ij}^d$ to t_{ij}^d since no ACK frames are transmitted. Moreover, plain FC can simply be implemented by setting $L_A = 0$ bits. As a summary, transmission and reception energies for plain FC in a single round are modified from Eqs. (10) and (14) as

$$\begin{aligned} E_{ij}^{tx}(l,k) = {} & E_{ij}^{enc}(l) + P_{tx}(l)N_{ij}^*(l)t_D \\ & + P_{std}[t_{ij}^s(l,k) - N_{ij}^*(l)t_D]. \end{aligned} \tag{16}$$

$$\begin{aligned} E_{ji}^{rx}(l,k) = {} & E^{dec}(M) + P_{rx}N_{ij}^*(l)t_D \\ & + P_{std}[t_{ji}^s(l,k) - N_{ij}^*(l)t_D]. \end{aligned} \tag{17}$$

3) Plain ARQ: In plain ARQ, frame exchange between any two-node pair is achieved through a two-way handshake mechanism where each successfully delivered data frame should be acknowledged successfully [46]. There are three possible cases for the two-way handshaking mechanism: (i) successful handshake (*i.e.*, data and ACK frames are successfully delivered), (ii) ACK frame errors (*i.e.*, data frame has received without an error, however, ACK frames are dropped in the reverse link), (iii) Data frame errors (*i.e.*, data frames are dropped in the forward link, hence no ACK frames are transmitted). For the cases (ii) and (iii), the handshaking should be repeated via retransmissions which incur extra energy dissipation.

Assume that node-i transmits a data frame to node-j with power level-l. As soon as the data frame is successfully received, an ACK frame is transmitted with power level-k by node-j. According to this transmission scheme, the probability of the handshaking to be successful is calculated as

$$p_{ij}^{HDS}(l,k) = [1 - p_{ij}^F(l,L_P)] \times [1 - p_{ji}^F(k,L_A)]. \tag{18}$$

The average number of transmissions required to attain a successful handshake is $\eta_{ij}(l,k) = \frac{1}{p_{ij}^{HDS}(l,k)}$. The slot time of the active phase for plain ARQ can be expressed as

$$t_{ij}^{s}(l,k) = (t'_D + 2t_{ij}^{d} + t_A) \times \eta_{ij}(l,k), \tag{19}$$

where $t'_D = \frac{L_P}{R}$ is the time required to transmit a data frame of $\frac{L_P}{R}$ bits and $2t_{ij}^{d}$ is the round-trip propagation delay encountered in both data and ACK frame transmissions. If the handshake is successful (*i.e.*, case (i)), then $p_{ij}^{HDS}(l,k) = \eta_{ij}(l,k) = 1$. Hence, the slot time of the active phase can be reduced to $t_{ij}^{s}(l,k) = (t'_D + 2t_{ij}^{d} + t_A)$. The energy consumed by the transmitter node-i in a successful handshake is calculated as

$$E_{tx,ij}^{HDS,s}(l,k) = P_{std}(2t_{ij}^{d}) + P_{tx}(l)t'_D + P_{rx}t_A, \tag{20}$$

where $P_{std}(2t_{ij}^{d})$, $P_{tx}(l)t'_D$, and $P_{rx}t_A$ are the energy dissipations for staying in the idle mode, transmitting a data frame, and receiving an ACK frame, respectively. On the other hand, if the handshake has failed due to the reasons stated in cases (ii) or (iii), then the handshake should be repeated. Therefore, the energy consumption of the transmitter node-i for the unsuccessful handshaking is given as

$$\begin{aligned} E_{tx,ij}^{HDS,f}(l,k) = &\underbrace{E_{tx,ij}^{HDS,s}(l,k) \times p_{ij}^{F}(l,L_P)\eta_{ij}(l,k)}_{\text{case (iii)}} \\ &+ \underbrace{E_{tx,ij}^{HDS,s}(l,k) \times \{[1-p_{ij}^{F}(l,L_P)]p_{ji}^{F}(k,L_A)\}\eta_{ij}(l,k)}_{\text{case (ii)}}, \end{aligned} \tag{21}$$

where $\{[1 - p_{ij}^{F}(l,L_P)]p_{ji}^{F}(k,L_A)\}\eta_{ij}(l,k)$ and $p_{ij}^{F}(l,L_P)\eta_{ij}(l,k)$ are the retransmission ratios required for the handshakes to be successful for cases (ii) and (iii), respectively. Hence, the total energy dissipation of the transmitter node-i in a single round is expressed as

$$E_{ij}^{tx}(l,k) = E_{tx,ij}^{HDS,s}(l,k) + E_{tx,ij}^{HDS,f}(l,k). \tag{22}$$

On the other hand, the receiver node-j consumes

$$E_{rx,ji}^{HDS,s}(l,k) = P_{std}(2t_{ij}^{d}) + P_{tx}(k)t_A + P_{rx}t'_D, \tag{23}$$

of energy for a successful handshake where $P_{std}(2t_{ij}^{d})$, $P_{tx}(k)t_A$, and $P_{rx}t'_D$ are the energy dissipations for staying in the idle mode, transmitting an ACK frame with power level-k, and receiving a data frame, respectively. If the handshaking is corrupted due to the case (ii), then the energy consumption of node-j is scaled as

$$\begin{aligned} E_{rx,ji}^{HDS,f_1}(l,k) = &E_{rx,ji}^{HDS,s}(l,k) \\ &\times \{[1-p_{ij}^{F}(l,L_P)]p_{ji}^{F}(k,L_A)\}\eta_{ji}(l,k). \end{aligned} \tag{24}$$

However, if the handshake has failed due to the reason stated in case (iii), the receiver node stays in the idle mode during the entire slot time since the receiver node would expect a data frame to be received. The energy dissipation of node-j in this case is given as

$$E_{rx,ji}^{HDS,f_2}(l,k) = P_{std} \times t_{ji}^{s} \times p_{ij}^{F}(l,L_P). \tag{25}$$

In overall, the total energy consumption of the receiver node-j in a single round is calculated as

$$E_{ji}^{rx}(l,k) = E_{rx,ji}^{HDS,s}(l,k) + E_{rx,ji}^{HDS,f_1}(l,k) + E_{rx,ji}^{HDS,f_2}(l,k). \tag{26}$$

C. ILP Framework for NL Maximization

The ILP framework is built on top of FC-ARQ, plain FC, and plain ARQ strategies and it aims to determine an optimum data flow routing plan for sensor nodes to convey their data to the base station in a manner that maximizes the NL [37], [38]. Hence, the NL maximization problem in this study has a convergecast (many-to-one) traffic. The classical definition of the NL (*i.e.*, number of rounds until the first node drains out its available battery [36]) has a drawback of energy efficiency such that some of the nodes (especially near to the base station) can drain their battery energies faster than other nodes. To avoid this problem, the ILP framework is constructed as a MaxMin problem such that we maximize the lifetime of the node which has the minimum lifetime. In this way, sensor nodes dissipate their battery energies in a balanced fashion such that all nodes collaborate to avoid the premature death of any individual node.

The objective function of the ILP framework is the maximization of NL (in s) which is defined in (27a) as $N_R \times T_R$ where N_R is the NL in terms of rounds. Constraints of the ILP framework are presented in (27b)–(27i). The set of all sensor nodes and all nodes (including the base station, node-1) are denoted by W and V, respectively. The set of directed links is represented as $\mathcal{E}$. The decision variables of the ILP framework are defined as

- f_{ij}^{m} (Integer Variable): The number of flows (which can contain a bulk of encoded frames of size L_P/M bits as in FC based FEC methods or a single unencoded frame of size L_P bits as in plain ARQ) originated from node-m flowing over link-(i,j) through the NL.
- T_{act}^{i} (Positive Cont. Variable): The total active phase duration of node-i during the NL (in s).
- E_i (Positive Cont. Variable): The total energy dissipation of sensor node-i during the NL (in Joules).
- N_R (Free Variable): NL in rounds.

$$\text{Maximize } N_R \times T_R \tag{27a}$$

subject to:

$$\sum_{\substack{j\in V \\ i\neq j}} f_{ij}^{m} - \sum_{\substack{j\in W \\ i\neq j}} f_{ji}^{m} = \begin{cases} N_R & \text{if } i = m \\ -N_R & \text{if } i = 1 \\ 0 & \text{o.w.} \end{cases}, \quad \forall i \in V, \forall m \in W \tag{27b}$$

$$\sum_{j\in W} f_{jm}^{m} = 0, \quad \forall m \in W \tag{27c}$$

$$T_{act}^{i} = \sum_{m\in W}\sum_{j\in V} f_{ij}^{m}(t_{ij}^{s})^{*} + \sum_{m\in W}\sum_{j\in W} f_{ji}^{m}(t_{ji}^{s})^{*}, \quad \forall i \in W \tag{27d}$$

$$T_{act}^{i} \leq N_R \times T_R, \ \forall i \in W \tag{27e}$$

$$\begin{aligned} &\sum_{m\in W}\sum_{j\in V} f_{ij}^{m}(E_{ij}^{tx})^{*} + \sum_{m\in W}\sum_{j\in W} f_{ji}^{m}(E_{ji}^{rx})^{*} \\ &+ P_{hbr} \times \left(N_R \times T_R - T_{act}^{i}\right) = E_i, \ \forall i \in W \end{aligned} \tag{27f}$$

$$E_i \leq \xi, \quad \forall i \in W \tag{27g}$$

$$f_{ij}^m = 0 \text{ if } d_{ij} > R_{max}, \quad \forall (i,j) \in \mathcal{E}, \forall m \in W \tag{27h}$$

$$f_{ij}^m \geq 0, \quad \forall (i,j) \in \mathcal{E}, \forall m \in W \tag{27i}$$

Const. (27b) is the per-node flow balance constraint which states that outgoing and incoming flows are balanced at each source node (*i.e.*, if $i = m$), base station (if $i = 1$), and relay nodes (*i.e.*, if $i \neq m$ and $i \neq 1$), respectively. In other words, this constraint ensures that only one flow is generated at each sensor node in each round. Hence, the total number of flows generated by each sensor node during the NL will be N_R. Const. (27c) prevents loops at each source node-m such that generated flows cannot be terminated at the source node-m. The total *active phase* duration of node-i during the NL is calculated in Const. (27d). Note that T_{act}^i is the summation of times required for both transmitting and receiving flows by each sensor node-i during the NL. In this constraint, $(t_{ij}^s)^*$ is the optimum slot time of the active phase for link-(i,j) which is obtained by plugging optimum transmission power levels used for both data frames (*i.e.*, l_{ij}^*) and ACK frames (*i.e.*, k_{ji}^*) into t_{ij}^s definition for the considered strategy. $\{l_{ij}^*, k_{ji}^*\}$ are determined such that the summation of energy dissipations for both transmissions and receptions over each link-(i,j) are minimized while at the same time $\{l_{ij}^*, k_{ji}^*\}$ should satisfy the targeted SNR criterion on each link-(i,j) (*i.e.*, $\overline{\gamma_{tgt}} = 20$ dB [7]) which can be expressed as [46]

$$\{l_{ij}^*, k_{ji}^*\} = \underset{l \in \mathcal{L}, k \in \mathcal{L}}{\operatorname{argmin}} \left(E_{ij}^{tx}(l,k) + E_{ji}^{rx}(l,k) \right). \tag{28}$$

Const. (27e) is the per-node bandwidth capacity constraint which states that the *active phase* duration of sensor node-i cannot be greater than the NL. Const. (27f) calculates the total amount of energy consumed by node-i during the NL (*i.e.*, E_i) which includes the total amount of energy required for transmission, reception, and hibernation through the NL. In this constraint, $(E_{ij}^{tx})^*$ and $(E_{ji}^{rx})^*$ are obtained in a similar way as $(t_{ij}^s)^*$. A sensor node switches to the *hibernation phase* for $(N_R \times T_R - T_{act}^i)$ s and consumes $P_{hbr} \times (N_R \times T_R - T_{act}^i)$ of energy where $P_{hbr} = 220$ μW is the power required for WHOI Micromodem to stay in hibernation phase [24]. Const. (27g) limits E_i to the initial battery (*i.e.*, $\xi = 100$ KJ). Const. (27h) defines the maximum communication range of sensor nodes (*i.e.*, $R_{max} = 2.5$ km [9]). Finally, Const. (27i) states that flows are non-negative.

FC-ARQ, plain FC, and plain ARQ strategies are employed by using the ILP framework presented in (27) such that $(t_{ij}^s)^*$, $(E_{ij}^{tx})^*$, and $(E_{ji}^{rx})^*$ parameters are adopted from

- Eqs. (8), (10), and (14) for FC-ARQ,
- Eqs. (15), (16), and (17) for plain FC,
- Eqs. (19), (22), and (26) for plain ARQ,

by plugging in l_{ij}^* and k_{ji}^* that are determined by Eq. (28).

In our framework, all nodes are assumed to be aware of their 3D coordinates by the aid of some localization services [47]. Furthermore, we assume that the base station solves the ILP framework, performs data flow planning, and allocates time slots in a centralized manner since the base station, in general, has higher computation capacity and energy sources than ordinary sensor nodes [48].

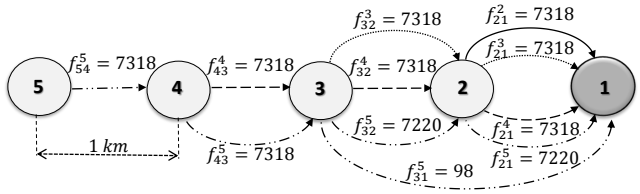

(a) Plain ARQ

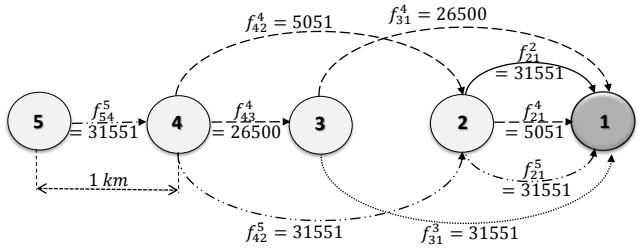

(b) FC-ARQ

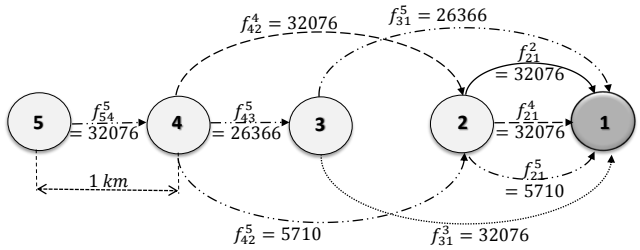

(c) Plain FC

Fig. 1: NLs (s) for all strategies in a five-node line network.

IV. Performance Evaluation

In this section, performances of FC-ARQ and plain FC strategies in terms of NL, end-to-end delay, energy consumption, and FER are compared against the performance of plain ARQ strategy. We construct the underwater channel model (Section III-A) and proposed strategies (Section III-B) in MATLAB while the ILP framework (Section III-C) is solved with GAMS using CPLEX 12 solver [49]. GAMS is a high-level mathematical programming and optimization tool that consists of a language compiler and high-performance solvers. GAMS/CPLEX 12 uses branch and cut algorithm to solve the ILP framework to optimality by solving a series of linear programming subproblems.

A. Toy Example

We present our results on a small-scale line topology in Fig. 1. In the line topology, 5 nodes with same depths are positioned such that the inter-node distance is 1 km. Node-1 is marked as the base station while nodes 2–5 are ordinary sensor nodes. We choose $L_P = 1024$ bits, $M = 4$, and $P_{tgt}^* = 0.999$ [17]. In each round, a single data flow (which contains a bulk of frames of size $L_P/M = 256$ bits as in FC based FEC methods or a single unencoded frame of size $L_P =$

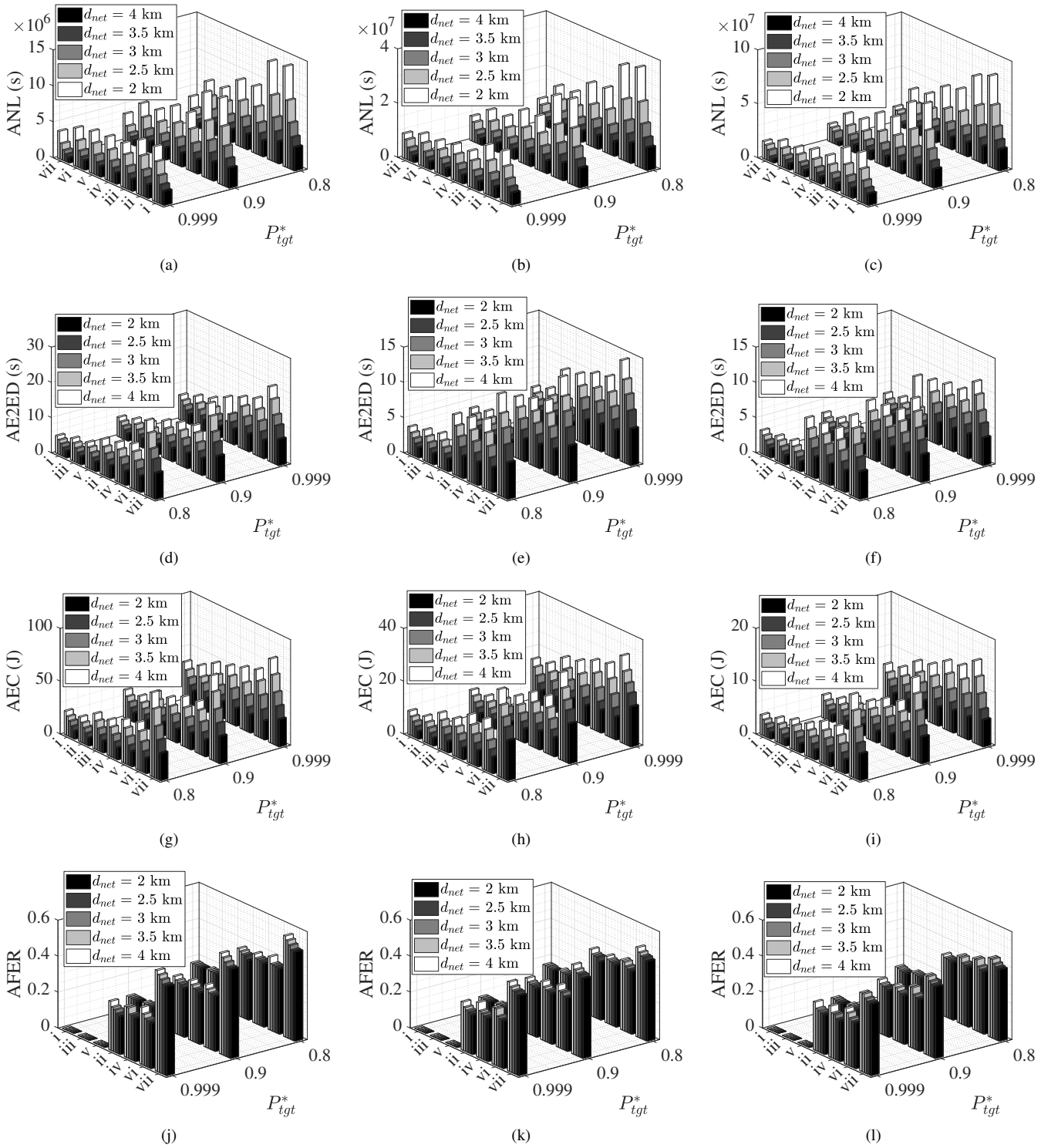

Fig. 2: Average network lifetimes (ANL) in s (first row), average end-to-end delays (AE2ED) in s (second row), average energy consumption (AEC) in Joules (third row), and average FERs (AFER) (last row) with respect to d_{net} and P^*_{tgt} when $L_P = 1024$ bits (first column), 512 bits (second column), and 256 bits (last column) for (i) Plain FC ($M = 4$), (ii) FC-ARQ ($M = 4$), (iii) Plain FC ($M = 2$), (iv) FC-ARQ ($M = 2$), (v) Plain FC ($M = 1$), (vi) FC-ARQ ($M = 1$), and (vii) Plain ARQ.

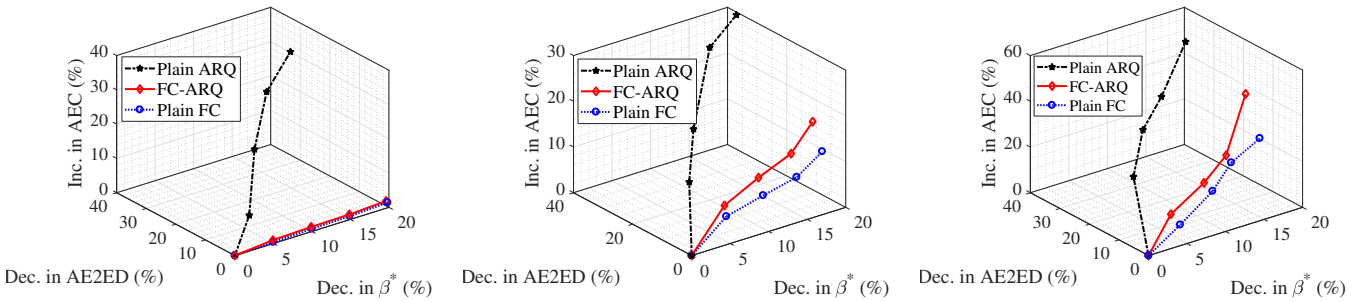

(a) $d_{net} = 2$ km (b) $d_{net} = 3$ km (c) $d_{net} = 4$ km

Fig. 3: Energy-delay trade-off as a function of decrement in β^* (percentage) for all strategies.

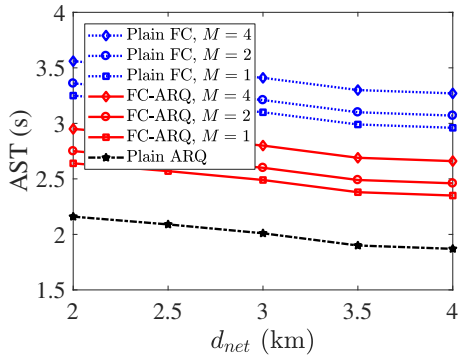

Fig. 4: Average solution times (AST) in s for all strategies.

1024 bits as in plain ARQ) is generated by sensor nodes. In each subfigure, we present optimum data flows (*i.e.*, f_{ij}^m) that maximize the NL for plain ARQ, FC-ARQ, and plain FC, respectively. Moreover, in each subfigure, solid, dotted, longdashed, and dotdashed line styles are used to represent optimum flow route plans for nodes 2, 3, 4, and 5, respectively.

In Fig. 1a, optimum data flows that maximize the NL for plain ARQ are shown. The NL is calculated as 7.32×10^5 s. Since each sensor node generates a single data flow (a single frame of 1024 bits) in each round, the total number of flows generated during the NL by each sensor node is 7318. In order to investigate the optimum flow route plans, we choose node-5 as an example. Node-5 transmits its generated flows to the base station in two different paths (*i.e.*, paths 5-4-3-1 and 5-4-3-2-1, respectively). The total number of flows conveyed in paths 5-4-3-1 and 5-4-3-2-1 are 98 and 7220, respectively. In this optimum flow route plan, a total number of 98+7220=7318 flows of node-5 are transmitted to the base station for maximizing the NL. A similar interpretation can also be applied for other sensor nodes.

In Fig. 1b, optimum flow route plans for FC-ARQ are shown. The NL of FC-ARQ is obtained as 3.16×10^6 s. Node-5 uses a single optimum path 5-4-2-1 where 31551 flows are conveyed to the base station. In Fig. 1c, results for plain FC are shown. The NL is calculated as 3.21×10^6 s. Node-5 has two optimum paths. The first path is 5-4-3-1 and the second path is 5-4-2-1 where 26366 and 5710 flows are conveyed in paths 5-4-3-1 and 5-4-2-1, respectively. Finally, our results reveal that when maximizing the NL, each sensor node dissipates at least 99.995% of its battery energy in a balanced fashion such that premature death of any sensor node is avoided.

B. Random Node Deployment

In this part, $|W| = 20$ sensor nodes are uniformly distributed in a square area of $d_{net} \times d_{net}$ m with depth $h = 1000$ m to simulate a deep network [50]. Sensor nodes have uniform depths and nodes are anchored to the bottom of the ocean. On the other hand, the base station is floating on the water surface and located at $(d_{net}, d_{net}, 0)$. We choose d_{net} between 2 km and 4 km with an increment of 500 m to investigate the impact of node density on proposed strategies. To analyze the effects of topological and channel changes, we consider 100 randomly generated networks and in each subsequent figure, we present the average results. For FC based FEC methods, we choose $M = 1$, 2, and 4 with three targeted reliability criteria (*i.e.*, $P_{tgt}^* = 0.8$, 0.9, and 0.999, respectively [17]). Moreover, we choose $L_P = 1024$, 512, and 256 bits. Note that when $L_P = 256$ bits and $M = 4$, the data frame size for FC based FEC methods and the ACK frame size are equal (*i.e.*, 64 bits).

1) Average Network Lifetime (ANL): In Figs. 2a, 2b, and 2c, we present ANLs in terms of s (in z-axis) for all strategies (in y-axis) with respect to (wrt.) P_{tgt}^* criteria (in x-axis) for the chosen d_{net}, L_P, and M values. In each subfigure, plain FC has the highest ANLs which are followed by FC-ARQ and plain ARQ for a fixed d_{net}, P_{tgt}^*, and M. For instance, in Fig. 2a when $d_{net} = 2$ km, $P_{tgt}^* = 0.8$, and $M = 2$, ANLs are obtained as 9.16×10^6 s, 9.03×10^6 s, and 3.81×10^6 s for plain FC, FC-ARQ, and plain ARQ, respectively. For a fixed L_P, the maximum possible ANLs are obtained for plain FC with $M = 4$ and $P_{tgt}^* = 0.8$ when $d_{net} = 2$ km. For example, maximum NLs are obtained as 1.39×10^7 s (when $L_P = 1024$ bits in Fig. 2a), 3.63×10^7 s (when $L_P = 512$ bits in Fig. 2b), and 8.39×10^7 s (when $L_P = 256$ bits in Fig. 2c), respectively.

Plain ARQ yields the lowest ANLs (7.19×10^5–1.60×10^7 s) for all the parameter configurations. Note that, P_{tgt}^* and M values do not have an impact on ANLs obtained for plain ARQ. On the other hand, FC based FEC methods can significantly prolong ANLs such that these approaches yield at least 16%–37% better ANLs than plain ARQ. Furthermore, ANLs decrease as d_{net} increases. Since network gets sparser,

link distances increase, hence sensor nodes consume more energy for communications which would result in low ANLs. As the reliability criterion is tightened (*i.e.*, high P^*_{tgt} values), ANL differences between plain FC and FC-ARQ increase. Plain FC results up to 21% prolonged ANLs than FC-ARQ as P^*_{tgt} is tightened from 0.8 to 0.999. The reason behind this result is due to the transmission of ACK frames which negatively effects ANLs in FC-ARQ. Our results show that higher M values yield extended ANLs for FC based FEC methods. Since the increment in M results in smaller frames to be transmitted, less energy is required for communications. Finally, decreasing L_P helps to improve ANLs.

2) Average End-to-End Delay (AE2ED): In Figs. 2d, 2e, and 2f, average end-to-end delays (AE2EDs) are shown. AE2ED is calculated by using the optimum slot times of the active phase for the links that contain flows (*i.e.*, $(t^s_{ij})^*$) as: $[\sum_{m\in W}\sum_{(i,j)\in\mathcal{E}} f^m_{ij}(t^s_{ij})^*]/[\sum_{m\in W}\sum_{(i,j)\in\mathcal{E}} f^m_{ij}]$.

AE2EDs can be as high as 21.16 s (in Fig 2d) and can be as low as 3.94 s (in Fig 2f) for plain ARQ. FC-ARQ and plain FC have AE2EDs in the intervals 3.07–15.83 s and 1.26–9.93 s, respectively. Note that plain FC has the lowest AE2EDs since no retransmissions are required for this strategy. Overall, these results indicate that FC based FEC methods can reduce AE2EDs at least by 11% when compared to plain ARQ for all the parameter space. AE2EDs rise as P^*_{tgt} increases for both FC-ARQ and plain FC when M is fixed. The reason behind this result is the increment in the number of redundant packets that are transmitted which greatly increases AE2EDs. Furthermore, for a fixed P^*_{tgt} value, AE2EDs decrease as M increases since smaller packets have low transmission times. As the network gets sparse, AE2EDs increase. Finally, reducing L_P from 1024 bits to 256 bits can further reduce AE2EDs up to 47%.

3) Average Energy Consumption (AEC): In Figs. 2g, 2h, and 2i, we present average energy consumptions (AECs) per node in a single round. AEC is calculated by dividing the sum of energy consumptions of all sensor nodes during the NL (*i.e.*, $\sum_{i\in W} E_i$) by the multiplication of number of nodes and NL (in rounds) (*i.e.*, $|W|\times N_R$) as: $[\sum_{i\in W} E_i]/[|W|\times N_R]$.

Plain ARQ has the highest AECs (*i.e.*, 5.08–79.24 J) as compared to FC based FEC methods. Moreover, FC based FEC methods can reduce AECs at least by 14% when compared to plain ARQ. Nevertheless, AECs for FC-ARQ and plain FC strategies are in the intervals 1.31–62.35 J and 1.20–57.69 J, respectively. Plain FC can further reduce AECs at most by 17% as compared to FC-ARQ for a fixed M. As the reliability criterion is tightened for a fixed M, more energy is dissipated for FC based FEC methods. On the other hand, for a fixed reliability criterion, increasing M results in low energy dissipation for FC based FEC methods. As d_{net} increases, more energy is dissipated for communicating over long links which increases the overall energy consumption.

Utilization of shorter L_P values helps in to reduce AECs at least by 41%. Our results also show that each sensor node consumes at least 99.8363%, 99.9777%, and 99.9919% of its battery energy on the average when the NL is maximized for plain ARQ, FC-ARQ, and plain FC, respectively. Therefore, the NL maximization technique which is developed via the ILP framework proposed in (27) sufficiently characterizes the energy efficiency of the investigated strategies.

4) Average Frame Error Rate (AFER): In Figs. 2j, 2k, and 2l, we present average frame error rates (AFERs). We use the successful handshake probability defined in Eq. (18) to calculate AFERs for plain ARQ as

$$\frac{\sum_{m\in W}\sum_{(i,j)\in\mathcal{E}} f^m_{ij}[1-p^{HDS}_{ij}(l^*_{ij},k^*_{ji})]}{\sum_{m\in W}\sum_{(i,j)\in\mathcal{E}} f^m_{ij}}. \tag{29}$$

On contrary, the success rate of FC defined in Eq. (7) and FER of ACK frames (*i.e.*, $p^F_{ji}(k,L_A)$) are used to calculate AFERs for FC based FEC methods as

$$\frac{\sum_{m\in W}\sum_{(i,j)\in\mathcal{E}} f^m_{ij}[1-\{P^s_{ij}(l^*_{ij})\times(1-p^F_{ji}(k^*_{ji},L_A))\}]}{\sum_{m\in W}\sum_{(i,j)\in\mathcal{E}} f^m_{ij}}. \tag{30}$$

AFERs are highest for plain ARQ (in the interval 0.398–0.561). Moreover, FC-ARQ and plain FC can reduce AFERs at least by 9% and 60% as compared to plain ARQ. For example, FC-ARQ and plain FC have AFERs in the intervals 0.211–0.405, and 0.001–0.184, respectively. Since frame sizes are reduced from L_P to $\frac{L_P}{M}$ in FC based FEC methods, these methods have lower AFERs than plain ARQ. As the ACK frame transmissions are completely ignored in plain FC (*i.e.*, $p^F_{ji}(k^*_{ji},L_A)=0$), the term $[1-P^s_{ij}(l^*_{ij})\times(1-p^F_{ji}(k^*_{ji},L_A))]$ reduces to $[1-P^s_{ij}(l^*_{ij})]$ for plain FC. Since $[1-P^s_{ij}(l^*_{ij})\times(1-p^F_{ji}(k^*_{ji},L_A))]\geq[1-P^s_{ij}(l^*_{ij})]$, AFERs of plain FC are at least 4% less than FC-ARQ. Increasing M has a positive impact on to reduce AFERs for FC based FEC methods. Similarly, when P^*_{tgt} rises, $P^s_{ij}(l^*_{ij})$ also increases which would reduce AFERs for FC based FEC methods. Finally, our results show that as d_{net} increases, AFERs also increase.

5) Energy-Delay Trade-off: In this part, we investigate the energy-delay trade-off for the proposed strategies. Following the similar approach presented in [41], we use the hop count metric to explore the energy-delay trade-off. To calculate the total hop count in the network (*i.e.*, the number of hops required for all sensor nodes to reach the base station), the following constraints are introduced in (27).

$$\sum_{\substack{j\in V\\ i\neq j}} a^m_{ij} - \sum_{\substack{j\in W\\ i\neq j}} a^m_{ji} = \begin{cases} 1 & \text{if } i=m \\ -1 & \text{if } i=1 \\ 0 & \text{o.w.} \end{cases}, \quad \forall i\in V, \forall m\in W \tag{31a}$$

$$f^m_{ij}\leq a^m_{ij}\mathcal{M}, \quad \forall (i,j)\in\mathcal{E}, \forall m\in W \tag{31b}$$

$$\sum_{m\in W}\sum_{(i,j)\in\mathcal{E}} a^m_{ij}\leq\beta \tag{31c}$$

We define the binary variable a^m_{ij} as the flow indicator to calculate the hop count in the network (indeed, summation of a^m_{ij} yields the total hop count in the network). a^m_{ij} gets 1 if the link-(i,j) conveys the flow originated at node-m. Const. (31a) is used to balance the number of hops at each sensor node-i. Const. (31b) states that if the indicator variable is set to 1 (*i.e.*, $a^m_{ij}=1$) then there is a non-zero number of flows which has an upper bound of $\mathcal{M}$ (sufficiently a large number).

Otherwise, when $a_{ij}^m = 0$, then $f_{ij}^m = 0$. Const. (31c) bounds the total hop count in the network to the integer variable, β.

We first calculate β values for a given network configuration by solving the ILP framework in (27) with the additional constraints introduced in (31). We define the parameter, β^*, as the total hop count in the network which maximizes the NL. Then, we gradually reduce β^* by 5% to 20% and set the new reduced hop count value as β in Const. (31c). Note that, we limit the reduction of β^* up to 20% because after this point, the ILP framework cannot provide feasible solutions since sensor nodes nearly dissipate their battery energies in less than a single round. Finally, we solve the ILP framework given in (27) with the additional constraints defined in (31) by using the new reduced β values. In this case, β in Const. (31c) is treated as a parameter instead of a variable. When β is reduced, sensor nodes use paths which contain low number of hops. This routing solution reduces AE2EDs. On the other hand, more energy is consumed by sensor nodes due to the increment in link distances.

Fig. 3 shows the increment in AECs as percentage (in *z*-axis) and the decrement in AE2EDs as percentage (in *y*-axis) when β^* is reduced by 0%–20% (in *x*-axis). We fix $L_P =$ 1024 bits and consider three d_{net} values (*i.e.*, 2, 3, and 4 km, respectively). Moreover, we choose $M = 4$ with $P_{tgt}^* = 0.999$ to investigate the energy-delay trade-off for nearly reliable networks. When β^* is not reduced (*i.e.*, 0%), there are no changes in either AE2EDs or AECs. As the reduction in β^* increases, both decrements in AE2EDs and increments in AECs increase. The changes in AE2EDs and AECs also increase as network gets sparse (high d_{net} values). Plain ARQ is the most affected strategy as the hop count in the network is reduced since this strategy has the highest AE2EDs and AECs as compared to FC based FEC methods. AE2EDs are reduced by 8%–40% while AECs are increased by 4%–45% for plain ARQ. Drops in AE2EDs are observed at most by 19% and 14% for FC-ARQ and plain FC, respectively. On the other hand, AECs are increased at most by 36% and 20% for FC-ARQ and plain FC, respectively.

6) Time Complexity Analysis: In Fig. 4, average solution times (ASTs) to obtain optimum solutions for the ILP framework are presented as a function of d_{net}. In this figure, solution times are averaged for all possible configurations of L_P and P_{tgt}^* values. ASTs are lowest for plain ARQ (1.87–2.16 s) which are followed by FC-ARQ (2.35–2.95 s), and plain FC (2.96–3.56 s), respectively. Due to the computation of P_{tgt}^* values in FC based FEC methods, the ILP framework requires more time to determine the optimum paths to maximize the NL for plain FC and FC-ARQ as compared to plain ARQ. Moreover, as M rises, ASTs increase for both FC-ARQ and plain FC because the number of links with low FERs increases which would expand the search space of the ILP framework (thus increasing ASTs) since these low FER links are possible candidates for flows to be conveyed. This is also the reason that ASTs for plain FC are greater than ASTs for FC-ARQ. Finally, As d_{net} decreases, more link options with low FERs would increase ASTs of the ILP framework.

V. Conclusion

In this study, we compare the performances of FC based FEC methods against classical ARQ in terms of NL, end-to-end delay, energy consumption, and FER for UASNs. Our main conclusions are enumerated as follows:

1) Classical ARQ can guarantee per packet transmission reliability, however it has worse performance metrics when compared to FC based FEC methods.
2) FC-ARQ can extent the NL at a minimum of 16% while decreasing the average end-to-end delays, energy consumptions, and FERs at least by 11%, 14%, and 9%, respectively as compared to plain ARQ.
3) For time-critical UASNs, plain FC is the best choice among other strategies such that this strategy can further reduce the average end-to-end delays up to 69% as compared to FC-ARQ. Nonetheless, NLs can be prolonged by up to 21% while average energy consumptions can be reduced at most 17% for plain FC as compared to FC-ARQ. Moreover, average FERs of plain FC are at least 4% lesser than FC-ARQ.
4) For both FC based FEC methods, relaxing the reliability criterion yields further prolonged NLs, reduced average end-to-end delays, energy consumptions, and FERs.
5) It is suggested to fragment the original data frame when using an FC based FEC method. Our results reveal that fragmenting the original message frame into four sections (*i.e.*, $M = 4$) provides the best performance metrics. Similarly, using shorter data frames yields further improved performance metrics.
6) Limiting the total hop count in the network by 20% results up to 40%, 19%, and 14% reductions in average end-to-end delays; at most 45%, 36%, and 20% increments in average energy consumptions for plain ARQ, FC-ARQ, and plain FC, respectively.
7) Performance comparison of FC based FEC methods against plain ARQ can be performed by using the proposed ILP framework in less than 3.56 s on the average.

References

[1] G. Han, C. Zhang, L. Shu, and J. J. P. C. Rodrigues, "Impacts of deployment strategies on localization performance in underwater acoustic sensor networks," *IEEE T. Ind. Electron.*, vol. 62, no. 3, pp. 1725–1733, 2015.

[2] J. Jiang, G. Han, L. Shu, S. Chan, and K. Wang, "A trust model based on cloud theory in underwater acoustic sensor networks," *IEEE T. Ind. Inform.*, vol. 13, no. 1, pp. 342–350, 2017.

[3] Z. Zhou, W. Fang, J. Niu, L. Shu, and M. Mukherjee, "Energy-efficient event determination in underwater WSNs leveraging practical data prediction," *IEEE T. Ind. Inform.*, vol. 13, no. 3, pp. 1238–1248, 2017.

[4] I. Jawhar, N. Mohamed, J. Al-Jaroodi, and S. Zhang, "An architecture for using autonomous underwater vehicles in wireless sensor networks for underwater pipeline monitoring," *IEEE T. Ind. Inform.*, pp. 1–1, 2018.

[5] Z. Zhou, H. Mo, Y. Zhu, Z. Peng, J. Huang, and J. H. Cui, "Fountain code based adaptive multi-hop reliable data transfer for underwater acoustic networks," in *Proc. IEEE Int. Conf. on Commun. (ICC)*, 2012, pp. 6396–6400.

[6] Y. Xing and C. Tapparello, "Dynamic fountain codes for energy efficient data dissemination in underwater sensor networks," in *Proc. OCEANS 2017 - Anchorage*, 2017, pp. 1–6.

[7] D. H. Simao, B. S. Chang, G. Brante, R. D. Souza, F. A. de Souza, and M. E. Pellenz, "Energy consumption analysis of underwater acoustic networks using fountain codes," in *Proc. MTS/IEEE OCEANS - Monterey*, 2016, pp. 1–4.

[8] Y. Cui, J. Qing, Q. Guan, F. Ji, and G. Wei, "Stochastically optimized fountain-based transmissions over underwater acoustic channels," *IEEE T. Veh. Technol.*, vol. 64, no. 5, pp. 2108–2112, 2015.

[9] H. Wang, S. Wang, and E. Zhang, "An improved data transport protocol for underwater acoustic sensor networks," in *Proc. MTS/IEEE OCEANS - Monterey*, 2016, pp. 1–5.

[10] X. Du, K. Li, X. Liu, and Y. Su, "RLT code based handshake-free reliable MAC protocol for underwater sensor networks," *J. Sensors*, vol. 2016, no. 3184642, pp. 1–11, 2016.

[11] W. Chen, H. Yu, Q. Guan, F. Ji, and F. Chen, "Reliable and opportunistic transmissions for underwater acoustic networks," *IEEE Network*, pp. 1–6, 2018.

[12] H. Mo, A. C. Mingir, H. Alhumyani, Y. Albayram, and J. H. Cui, "UW-HARQ: An underwater hybrid ARQ scheme: Design, implementation and initial test," in *Proc. Oceans*, 2012, pp. 1–5.

[13] D. J. C. MacKay, "Fountain codes," *IEE Proc. - Commun.*, vol. 152, no. 6, pp. 1062–1068, 2005.

[14] H. Wang, S. Wang, E. Zhang, and J. Zou, "A network coding based hybrid ARQ protocol for underwater acoustic sensor networks," *Sensors*, vol. 16, no. 9, Article No: 1444, 2016.

[15] R. Ahmed and M. Stojanovic, "Random linear packet coding for fading channels," in *Proc. OCEANS - San Diego*, 2013, pp. 1–6.

[16] P. Xie, Z. Zhou, Z. Peng, J.-H. Cui, and Z. Shi, "SDRT: A reliable data transport protocol for underwater sensor networks," *Ad Hoc Netw.*, vol. 8, no. 7, pp. 708–722, 2010.

[17] G. Barreto, D. H. Simao, M. E. Pellenz, R. D. Souza, E. Jamhour, M. C. Penna, G. Brante, and B. S. Chang, "Energy-efficient channel coding strategy for underwater acoustic networks," *Sensors*, vol. 17, no. 4, Article No: 728, 2017.

[18] P. Casari, M. Rossi, and M. Zorzi, "Towards optimal broadcasting policies for HARQ based on fountain codes in underwater networks," in *Proc. Conf. on Wirel. on Demand Netw. Sys. and Serv.*, 2008, pp. 11–19.

[19] ——, "Fountain codes and their application to broadcasting in underwater networks: Performance modeling and relevant tradeoffs," in *Proc. ACM Int. Workshop on Underwater Netw. (WuWNeT)*, 2008, pp. 11–18.

[20] R. Diamant and L. Lampe, "Adaptive error-correction coding scheme for underwater acoustic communication networks," *IEEE J. Oceanic Eng.*, vol. 40, no. 1, pp. 104–114, 2015.

[21] R. Ahmed and M. Stojanovic, "Reliable communication using packet coding for underwater acoustic channels," in *Proc. IEEE Int. Workshop on Signal Proc. Advances in Wirel. Commun. (SPAWC)*, 2016, pp. 1–5.

[22] ——, "Joint power and rate control for packet coding over fading channels," *IEEE J. Oceanic Eng.*, vol. 42, no. 3, pp. 697–710, 2017.

[23] R. A. R. Ahmed and M. Stojanovic, "Random linear packet coding for high speed acoustic communication: An experimental analysis," in *Proc. Oceans - Yeosu*, 2012, pp. 1–7.

[24] L. Freitag, M. Grund, S. Singh, J. Partan, P. Koski, and K. Ball, "The WHOI micro-modem: an acoustic communications and navigation system for multiple platforms," in *Proc. MTS/IEEE OCEANS*, vol. 2, 2005, pp. 1086–1092.

[25] S. Jiang, "On reliable data transfer in underwater acoustic networks: A survey from networking perspective," *IEEE Commun. Surv. Tut.*, vol. 20, no. 2, pp. 1036–1055, 2018.

[26] N. Z. Zenia, M. Aseeri, M. R. Ahmed, Z. I. Chowdhury, and M. S. Kaiser, "Energy-efficiency and reliability in MAC and routing protocols for underwater wireless sensor network: A survey," *J. Netw. Comput. Appl.*, vol. 71, pp. 72–85, 2016.

[27] R. Bassoli, H. Marques, J. Rodriguez, K. W. Shum, and R. Tafazolli, "Network coding theory: A survey," *IEEE Commun. Surv. Tut.*, vol. 15, no. 4, pp. 1950–1978, 2013.

[28] M. Luby, "LT codes," in *Proc. IEEE Symp. on Found. of Comp. Sci.*, 2002, pp. 271–280.

[29] A. Shokrollahi, "Raptor codes," *IEEE T. Inform. Theory*, vol. 52, no. 6, pp. 2551–2567, 2006.

[30] R. Cao and L. Yang, "Robust data-centric storage for underwater acoustic sensor networks," in *Proc. OCEANS 2009*, 2009, pp. 1–7.

[31] ——, "Reliable transport and storage protocol with fountain codes for underwater acoustic sensor networks," in *Proc. ACM Int. Workshop on UnderWater Netw. (WUWNet)*, 2010, pp. 14:1–14:4.

[32] ——, "Decomposed raptor codes for data-centric storage in underwater acoustic sensor networks," in *Proc. MTS/IEEE OCEANS - Seattle*, 2010, pp. 1–9.

[33] ——, "Reliable relay-aided underwater acoustic communications with hybrid DLT codes," in *Proc. Military Commun. Conf. (MILCOM)*, 2011, pp. 412–417.

[34] C. Y. M. Chan and M. Motani, "An integrated energy efficient data retrieval protocol for underwater delay tolerant networks," in *Proc. OCEANS - Europe*, 2007, pp. 1–6.

[35] M. Liang, J. Duan, D. Zhao, J. Si, and X. Song, "Novel joint encoding/decoding algorithms of fountain codes for underwater acoustic communication," *J. Syst. Eng. Electron.*, vol. 27, no. 4, pp. 772–779, 2016.

[36] H. Yetgin, K. T. K. Cheung, M. El-Hajjar, and L. H. Hanzo, "A survey of network lifetime maximization techniques in wireless sensor networks," *IEEE Commun. Surv. Tut.*, vol. 19, no. 2, pp. 828–854, 2017.

[37] A. Ibrahim and A. Alfa, "Optimization techniques for design problems in selected areas in WSNs: A tutorial," *Sensors*, vol. 17, no. 8, 2017.

[38] R. M. Curry and J. C. Smith, "A survey of optimization algorithms for wireless sensor network lifetime maximization," *Comput. Ind. Eng.*, vol. 101, pp. 145–166, 2016.

[39] Z. Fei, B. Li, S. Yang, C. Xing, H. Chen, and L. Hanzo, "A survey of multi-objective optimization in wireless sensor networks: Metrics, algorithms, and open problems," *IEEE Commun. Surv. Tut.*, vol. 19, no. 1, pp. 550–586, 2017.

[40] J. U. Khan and H. S. Cho, "A data gathering protocol using AUV in underwater sensor networks," in *Proc. OCEANS - TAIPEI*, 2014, pp. 1–6.

[41] M. Felemban and E. Felemban, "Energy-delay tradeoffs for underwater acoustic sensor networks," in *Proc. Int. Black Sea Conf. on Commun. and Netw. (BlackSeaCom)*, 2013, pp. 45–49.

[42] F. Fazel, M. Fazel, and M. Stojanovic, "Random access compressed sensing over fading and noisy communication channels," *IEEE T. Wirel. Commun.*, vol. 12, no. 5, pp. 2114–2125, 2013.

[43] M. Gao, C. H. Foh, and J. Cai, "On the selection of transmission range in underwater acoustic sensor networks," *Sensors*, vol. 12, no. 4, pp. 4715–4729, 2012.

[44] C. Zidi, F. Bouabdallah, and R. Boutaba, "Routing design avoiding energy holes in underwater acoustic sensor networks," *Wirel. Commun. Mob. Com.*, vol. 16, no. 14, pp. 2035–2051, 2016.

[45] J. J. Kartha and L. Jacob, "Network lifetime-aware data collection in underwater sensor networks for delay-tolerant applications," *Sādhanā*, vol. 42, no. 10, pp. 1645–1664, 2017.

[46] H. U. Yildiz, V. C. Gungor, and B. Tavli, "Packet size optimization for lifetime maximization in underwater acoustic sensor networks," *IEEE T. Ind. Inform.*, pp. 1–1, 2018.

[47] M. Erol-Kantarci, H. T. Mouftah, and S. Oktug, "A survey of architectures and localization techniques for underwater acoustic sensor networks," *IEEE Commun. Surv. Tut.*, vol. 13, no. 3, pp. 487–502, 2011.

[48] P. Jiang, J. Liu, F. Wu, J. Wang, and A. Xue, "Node deployment algorithm for underwater sensor networks based on connected dominating set," *Sensors*, vol. 16, no. 3:388, 2016.

[49] GAMS Development Corporation, "General Algebraic Modeling System (GAMS) Release 24.2.1," Washington, DC, USA, 2013. [Online]. Available: http://www.gams.com/

[50] S. M. Ghoreyshi, A. Shahrabi, and T. Boutaleb, "An underwater routing protocol with void detection and bypassing capability," in *Proc. IEEE Int. Conf. Advanced Inf. Netw. and Appl. (AINA)*, 2017, pp. 530–537.

Huseyin Ugur Yildiz (S'13-M'16) received the B.S. degree from Bilkent University, Ankara, Turkey, in 2009; the M.S. and Ph.D. degrees from TOBB University of Economics and Technology, Ankara, Turkey, in 2013 and 2016, respectively, all in electrical and electronics engineering. He is an Assistant Professor in the Department of Electrical and Electronics Engineering at TED University, Ankara, Turkey. His research focuses on the applications of optimization techniques for modeling and analyzing research problems on wireless communications, wireless networks, underwater acoustic networks, and smart grids.